Compressive Holography

David J. Brady, Kerkil Choi, Daniel L. Marks, Ryoichi Horisaki and Sehoon Lim

Department of Electrical and Computer Engineering and The Fitzpatrick Institute for Photonics,
Duke University, Durham, NC 27708.

David.Brady@duke.edu

Abstract: Compressive sampling enables signal reconstruction using less than one measurement per reconstructed signal value. Compressive measurement is particularly useful in generating multidimensional images from lower dimensional data. We demonstrate single frame 3D tomography from 2D holographic data.

OCIS codes: (090.1995) Digital holography; (070.0070) Fourier optics and signal processing.

References and links

1. C. E. Shannon, "Communications in the presence of noise," in Proc.of the IREv **37,** 10–21 (1949).
2. M. Golay, "Multislit spectroscopy," J. Opt. Soc. Am. **39,** 437–444 (1949).
3. E. J. Candes, J. K. Romberg, and T. Tao, "Stable signal recovery from incomplete and inaccurate measurements," Communications on Pure and Applied Mathematics **59,** 1207–1223 (2006).
4. E. J. Candes and T. Tao, "Near-optimal signal recovery from random projections: Universal encoding strategies?," IEEE Transactions on Information Theory **52**(12), 5406–5425 (2006).
5. D. L. Donoho, "Compressed sensing," IEEE Transactions on Information Theory **52**(4), 1289–1306 (2006).
6. D. Takhar, J. N. Laska, M. B. Wakin, M. F. Duarte, D. Baron, S. Sarvotham, K. F. Kelly, and R. G. Baraniuk, "A new compressive imaging camera architecture using optical-domain compression," in *Computational Imaging IV*, **6065,** (San Jose, CA, USA), p. 606509, SPIE, 2006.
7. M. E. Gehm, R. John, D. J. Brady, R. M. Willett, and T. J. Schulz, "Single-shot compressive spectral imaging with a dual-disperser architecture," Opt. Express **15**(21), 14013–14027 (2007).
8. A. Wagadarikar, R. John, R. Willett, and D. J. Brady, "Single disperser design for coded aperture snapshot spectral imaging," Appl. Opt. **47**(10), B44–B51 (2008).
9. D. Gabor, "A new microscopic principle," Nature **161,** 777–778 (1948).
10. E. N. Leith and J. Upatnieks, "Reconstructed wavefronts and communication theory," J. Opt. Soc. Am. **52,** 1123–1130 (1962).
11. S. Seo, T. W. Su, D. K. Tseng, A. Erlinger, and A. Ozcan, "Lensfree holographic imaging for on-chip cytometry and diagnostics," Lab on a Chip **9**(6), 777–787 (2009).
12. W. Jueptner and U. Schnars, *Digital Holography*, (New York, Springer-Verlag, Berlin Heidelberg, 2005).
13. T. C. Poon, *Digital holography and three-dimensional display*, (New York; London: Springer, 2006).
14. M. E. Brezinski, *Optical coherence tomography*. (Amsterdam; Boston: Academic Press, 2006).
15. D. L. Marks, R. A. Stack, D. J. Brady, D. C. Munson, and R. B. Brady, "Visible cone-beam tomography with a lensless interferometric camera," Science **284**(5423), 2164–2166 (1999).
16. J. Sharpe, U. Ahlgren, P. Perry, B. Hill, A. Ross, and J. Hecksher-Sorensen, R. Baldock, and D. Davidson, "Optical projection tomography as a tool for 3d microscopy and gene expression studies," Science **296**(5567), 541–545 (2002).
17. A. J. Devaney, "Nonuniqueness in the inverse scattering problem," Journal of Mathematical Physics **19**(7), 1526–1531 (1978).
18. A. J. Devaney, "Geophysical diffraction tomography," IEEE Transactions on Geoscience and Remote Sensing **GE-22**, 3–13 (1984).
19. W. L. Chan, M. L. Moravec, R. G. Baraniuk, and D. M. Mittleman, "Terahertz imaging with compressed sensing and phase retrieval," Opt. Lett. **33**(9), 974–976 (2008).
20. I. Yamaguchi, K. Yamamoto, G. A. Mills, and M. Yokota, "Image reconstruction only by phase data in phase-shifting digital holography," Appl. Opt. **45**(5), 975–983 (2006).

#111469 - $15.00 USD Received 18 May 2009; revised 2 Jul 2009; accepted 5 Jul 2009; published 15 Jul 2009

21. R. Baraniuk and P. Steeghs, "Compressive radar imaging," IEEE Radar Conference, pp. 128-133, April, (2007).
22. L. Li, W. Zhang, F. Li, "Compressive diffraction tomography for Weakly Scattering," Submitted to IEEE Trans. on Geosciences and Remote Sensing (2009).
23. D. L. Donoho and M. Elad, "Optimally sparse representation in general (nonorthogonal) dictionaries via ℓ_1 minimization," Proceedings of the National Academy of Sciences of the United States of America, **100**(5), 2197–2202 (2003).
24. R. E. Blahut, *Theory of Remote Image Formation*, (Cambridge University Press, 2004).
25. J. W. Goodman, *Introduction to Fourier optics, 3rd Ed.*, (Roberts and Company Publishers, 2005).
26. D. M. Paganin, *Coherent X-ray Optics*, (Oxford Science Publications, 2006).
27. A. C. Kak and M. Slaney, *Principle of Computerized Tomographic Imaging*, (Society for Industrial and Applied Mathematics, 2001).
28. D. J. Brady, *Optical Imaging and Spectroscopy*, (Wiley, 2009).
29. L. I. Rudin, S. Osher, and E. Fatemi, "Nonlinear total variation based noise removal algorithms," Physica D **60**(1-4), 259–268 (1992).
30. J. M. Bioucas-Dias and M. A. T. Figueiredo, "A new twist: Two-step iterative shrinkage/thresholding algorithms for image restoration," , IEEE Transactions on Image Processing **16**, 2992–3004 (2007).
31. V. Micó, J. García, Z. Zalevsky, and B. Javidi, "Phase-shifting Gabor holography," Opt. Express **17**, 1492–1494 (2009).
32. T. Latychevskaia and H. W. Fink, "Solution to the Twin Image Problem in Holography," Phys. Rev. Lett. **98**, 233901 (2007).

1. Introduction

Studies presented in 1949 by Shannon and Golay have recently collided in a major revision to signal and image measurement theory. Shannon is traditionally cited to support the claim that the sampling rate in a high fidelity imaging system must be greater than twice the spatial bandwidth [1]. Golay introduced the idea of artificial discrete multiplex coding in optical measurements [2]. Candés, Tao and Romberg [3, 4] and Donoho [5] have demonstrated that signals, assumed to be sparse in some basis, sampled by multiplex encodings may be accurately infered with high probability using many fewer measurements than suggested by Shannon's sampling theorem. Takhar *et al.* applied compressive sampling algorithms in demonstrating a single pixel camera [6]. We have previously applied these methods with Golay-inspired coded aperture spectroscopy to demonstrate compressive measurement of 3D spectral datacubes from 2D measurements [7, 8].

This paper explores the relationship between compressive sampling and a third paper from the late 1940's, Gabor's invention of holography [9]. Gabor holography is an amazingly simple and effective encoder for compressive sampling. Decompressive inference improves holographic systems by increasing the number of pixels or voxels one can infer from a single hologram and by resolving reconstruction ambiguities. Holography is a comparatively effective encoder for compressive imaging because holographic multiplex measurement weights are complex valued.

After the invention of the laser, Gabor holography was generally supplanted by off-axis Leith-Upatnieks holograpy[10]. Signal reconstruction from off-axis holograms may be understood simply using Shannon sampling and linear filtering theory. As illustrated by recent studies of holographic cytometry [11], however, the simplicity of the Gabor geometry remains attractive and competitive. We demonstrate in this paper that interference terms that may not be removed from Gabor holograms by linear filtering may be removed by imposing a sparsity constraint.

Computational imaging from electronically recorded holograms recorded on electronic detector arrays is called digital holography [12, 13]. Digital holography typically relies on monochromatic laser illumination. Optical coherence tomography is a closely related technique relying on multispectral illumination for 3D interferometric tomography [14]. Alternative approaches to optical 3D imaging include projection tomography [15, 16] and confocal microscopy. Digital holography is not regarded as a 3D tomographic imaging technique because

#111469 - $15.00 USD Received 18 May 2009; revised 2 Jul 2009; accepted 5 Jul 2009; published 15 Jul 2009

3D object estimation from coherent scattering data is ill-posed [17]. This problem is traditionally addressed by recording holograms of objects illuminated by a sequence of plane waves, which forms the basis of diffraction tomography [18].

Our main result is that decompressive inference enables 3D tomography from a single 2D monochromatic digital hologram. While this result is in apparent conflict with Devaney's proof that holographic tomography is ill-posed, the overthrow of Devaney's objection using a sparsity prior and convex optimization parallels the overthrow of Shannon sampling by similar methods.

Our results also suggest that holography may have general advantages in compressive optical imaging. Since the irradiance is the only observable in conventional optical imaging, multiplex measurement codes are constrained to nonnegative weights. This results in relatively poor measurement conditioning. Holography, in contrast, is an interferometric modality in which both the amplitude and the phase of a field can be obtained as in radar or MRI. The complex-valued encodings may provide a more direct application of compressive sensing. Chan *et al.* [19] have previously described phase-sensitive terahertz compressive imaging.

We note that our approach is fundamentally different than hologram data compression [20]. Our approach is to directly collect a smaller number of measurements than the number of voxels (or pixels) in the reconstructions, whereas the hologram data compression applies data compression to the holograms that are already obtained. The word "compressive" in this paper emphasizes that our holographic sampling or sensing process encodes and compresses 3D datacube information into 2D holographic measurements. This encoding is inverted using compressive sampling theory [4, 5]. Similar terminology appears in related studies [21, 22].

2. Compressive sensing background

Compressive sensing theory ensures highly accurate reconstruction for multiplex encoders that satisfy a sufficient condition called the restricted isometry property (RIP) [3, 4]. Let a S-sparse signal be defined by a signal that has only S nonzero components and $(N-S)$ coefficients that are exactly zero. A matrix $H \in \mathbb{R}^{M\times N}$ is said to satisfy S-RIP with constant $\delta_S \in (0,1)$ if, for any S-sparse f,

$$(1-\delta_S)\|f_T\|_2^2 \leq \|H_T f_T\|_2^2 \leq (1+\delta_S)\|f_T\|_2^2, \tag{1}$$

where T denotes the set of indices on which the S-sparse signal is supported, and $\|\cdot\|_2$ denotes the Euclidean norm. This condition implies that for any S-sparse object to be reconstructed accurately and reliably, the corresponding sub-matrix H_T of H composed of S columns of H has to form a nearly isometry transformation. Note that the condition also implies that all the eigenvalues of the Gram matrix of any S-column sub-matrix H_T are distributed near 1 (in fact in the range of $[1-\delta_S\ 1+\delta_S]$), which consequently ensures that any S-column sub-matrix H_T is well-conditioned.

Let $\mu_1(H,\Psi)$ be defined by

$$\mu_1(H,\Psi) = \sqrt{N} \max_{\substack{1\leq m\leq M \\ 1\leq n\leq N}} |\langle h_m, \psi_n\rangle|, \tag{2}$$

where h_m and ψ_n denote the m-th row of H and the n-th column of Ψ, respectively. Candés *et al.* [3] and Donoho [5] showed that if f is S-sparse in Ψ, and M satisfies

$$M \geq C \cdot \mu_1^2(H,\Psi) \cdot S \cdot \log N, \tag{3}$$

then an accurate reconstruction can be obtained with high probability by solving

$$\theta_e = \arg\min_{\theta} ||\theta||_1 \text{ such that } g = Hf_e = H\Psi\theta_e, \tag{4}$$

#111469 - $15.00 USD Received 18 May 2009; revised 2 Jul 2009; accepted 5 Jul 2009; published 15 Jul 2009

where $||\theta||_1 = \sum_i |\theta_i|$. S denotes the number of nonzero (or significant) coefficients of f in the Ψ domain. As clear from Eqn. (3), the smaller μ_1 is, the more accurate the reconstruction would be for the same M.

An alternative definition of coherence is given by

$$\mu_2(D) = \max_{i \neq j, 1 \leq i,j \leq N} \left\{ \frac{d_i^T d_j}{\|d_i\|_2 \|d_j\|_2} \right\}, \tag{5}$$

where d_i is the i-th column of the sensing matrix $D = H\Psi$. This can also be interpreted as the maximum off-diagonal element of the Gram matrix of D, whose columns are normalized. When $\mu_2(D)$ is minimal such that

$$S < \frac{1}{2}\left(1 + \frac{1}{\mu_2(D)}\right), \tag{6}$$

then the S-sparse is necessarily the sparsest solution that satisfies $\min_\theta \|\theta\|_0$, and hence can be obtained by solving Eqn. (4) [23].

Note that for $\Psi = I$ with I being an identity matrix (i.e., the canonical basis), $\mu_1(H,I) = 1$ for a discrete Fourier transform (DFT) matrix H. Hence, the DFT matrix that generates Fourier samples distributed uniformly at random over the frequency domain satisfies the so-called restricted isometry property with high probability given that $M \geq CS \log N$ is satisfied. Our Gabor hologram multiplex encoder may be considered as 3D Fourier transform encoder. However, our Fourier samples are limited to a certain band volume, which may produce a relatively large μ_1, larger than 1 in general. Holographic measurements using illumination with multiple wavelengths and/or angles can provide the Fourier samples over a larger band volume improving μ_1 and, consequently, the RIP for our Gabor hologram multiplex encoder.

3. Theory and Methods

As illustrated in Fig. 1, a Gabor hologram is formed in interference between a plane wave A and a 3D object with scattering density $\eta(x',y',z')$. A 2D detector array records the irradiance

$$\begin{aligned} I(x,y) &= |A + E(x,y)|^2 \\ &= |A|^2 + |E(x,y)|^2 + A^* E(x,y) + A E^*(x,y), \end{aligned} \tag{7}$$

where the scattered field E is defined under the Born approximation as

$$E(x,y) = \iiint dx'dy'dz' \eta(x',y',z') h(x-x', y-y', z-z'), \tag{8}$$

where h is the product of $\exp(ikz)$ representing the phase delay at a distance z [24] and the inverse Fourier transform of the propagation transfer function $\exp(iz\sqrt{k^2 - k_x^2 - k_y^2})$ [25, Eqn. (3-74)]. Note that the squared field term $|E(x,y)|^2$ produces the autocorrelation of the Fourier transform of the field E in the Fourier domain. In Eqn. (7), the term $|A|^2$ is simply a constant, and hence the effect of $|A|^2$ can be removed by eliminating the DC term (the term at the origin) from the Fourier transform of the interference irradiance measurements $I(x,y)$. Also, we may assume that A is 1 without loss of generality. Then, we may proceed with $A^*E(x,y) + AE^*(x,y) + |E(x,y)|^2 = 2\mathrm{Re}\{E(x,y)\} + |E(x,y)|^2 = 2\mathrm{Re}\{E(x,y)\} + e(x,y)$. If we neglect the nonlinearity caused by $|E(x,y)|^2$ and regard $e(x,y)$ as model error, then Eqn. (7) represents a linear mapping between the object scattering density and measurement data.

Let a 3D object (i.e., the scattering potential) be denoted by $\eta(x',y',z')$ with the convention that $z' = 0$ at the detector plane. Let the sample spacings be $\Delta_x = \Delta_y = \Delta$. Also, let Δ_z be the

#111469 - $15.00 USD Received 18 May 2009; revised 2 Jul 2009; accepted 5 Jul 2009; published 15 Jul 2009

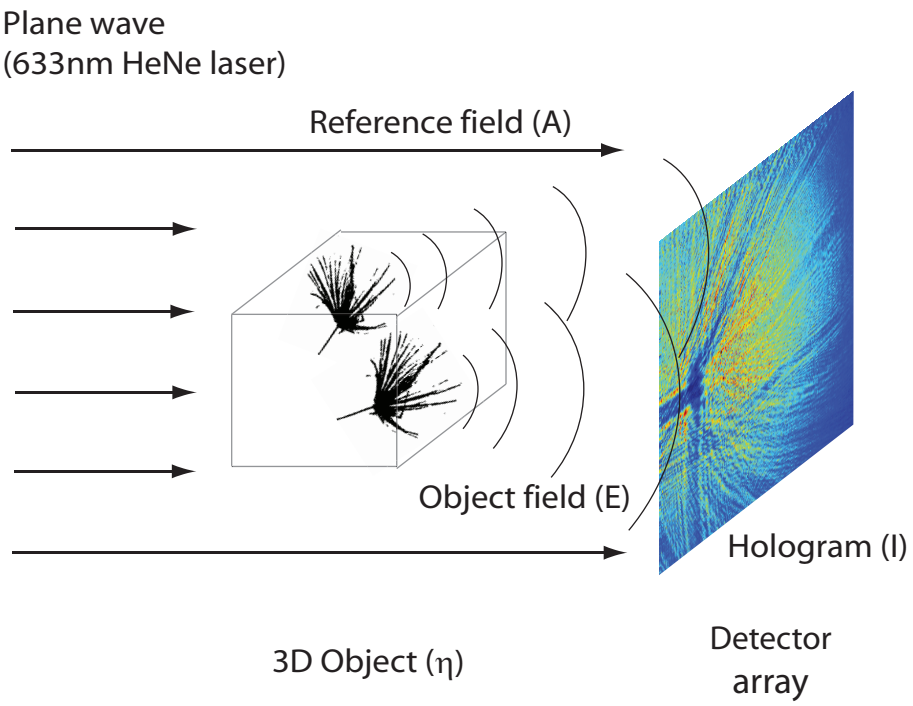

Fig. 1. Gabor hologram geometry.

sampling pitch in the z-axis. Let the number of pixels along each dimension of the detector be N. Using this notation, a 3D tomographic reconstruction problem may be formulated by noting the similarity of the data to that in diffraction tomography [24, 26]. Recall that the 2D field measurement $E(x,y)$ is related to the 3D object scattering density $\eta(x',y',z')$ through Eqn. (8). Therefore, a discrete mathematical forward model for tomographic reconstruction can be constructed by discretizing Eqn. (8).

The 2D sampled field at the detector plane with the sample spacings defined above can be expressed by

$$
\begin{aligned}
&E_{n_1 n_2} = E(n_1\Delta, n_2\Delta) \\
&= \frac{1}{(2\pi)^2}\int\cdots\int dz'dxdydk_xdk_y \iint dx'dy'\eta(x',y',z')e^{ikz'}e^{-i(k_xx'+k_yy')}\sum_{m_1'}\sum_{m_2'}\delta(x'-m_1'\Delta) \\
&\delta(y'-m_2'\Delta)e^{iz\sqrt{k^2-k_x^2-k_y^2}}\delta(z-z')e^{-i(k_xx+k_yy)}\delta(x-n_1\Delta)\delta(y-n_2\Delta)\sum_{m_1}\sum_{m_2}\delta(k_x-m_1\Delta_k) \\
&\delta(k_y-m_2\Delta_k)\sum_{l}\delta(z-l\Delta_z) \\
&= \frac{1}{N^2}\sum_{l}\sum_{m_1}\sum_{m_2}\left[\sum_{m_1'}\sum_{m_2'}\eta_{m_1'm_2'l}e^{-i2\pi\frac{m_1m_1'+m_2m_2'}{N}}\right]e^{ikl\Delta_z}e^{il\Delta_z\sqrt{k^2-m_1^2\Delta_k^2-m_2^2\Delta_k^2}}e^{-i2\pi\frac{n_1m_1+n_2m_2}{N}}, \quad (9)
\end{aligned}
$$

where $\eta_{m_1'm_2'l} = \eta(m_1'\Delta, m_2'\Delta, l\Delta_z)$. Note that the terms in the square bracket form the 2D discrete Fourier transform of η. Also note that the last exponential term in the last line of Eqn. (9)

#111469 - $15.00 USD Received 18 May 2009; revised 2 Jul 2009; accepted 5 Jul 2009; published 15 Jul 2009

also forms the inverse 2D Fourier transform in conjunction with the summations over m_1 and m_2. Hence, this equation can simply be written as

$$E_{n_1 n_2} = \mathscr{F}_{2D}^{-1}\left\{\sum_l \hat{\eta}_{m_1 m_2 l} e^{ikl\Delta_z} e^{il\Delta_z\sqrt{k^2-m_1^2\Delta_k^2-m_2^2\Delta_k^2}}\right\}, \tag{10}$$

where $\hat{\eta}$ denotes the Fourier transform of η, and $\mathscr{F}^{-1}$ denotes the inverse Fourier transform operator. Equation (10) is called a multislice approximation [26]. Eqn. (9) may also be viewed as a 2D slice of the 3D Fourier transform of η. The 2D slice can be interpreted as a surface patch of the Ewald *k*-sphere as in traditional diffraction tomography [27]. Note that while the 3D Fourier transform interpretation requires 3D interpolation of either the 3D Fourier transform of η or the 3D spatial scattering density η, the multiscale approximation requires no such interpolation and is less sensitive to errors that would result from 3D interpolation.

Define $\bar{g}_{(n_2-1)\times N_x+n_1} = E_{n_1,n_2}$ and $f_{(l-1)\times(N_x\times N_y)+(m_2'-1)\times N_x+m_1'} = \eta_{m_1',m_2',l}$, where N_x and N_y denote the numbers of pixels of the detector in the *x*-direction and *y*-direction, respectively. With these definitions, Eqn. (10) may be rewritten as

$$\bar{g} = G_{2D}QBf, \tag{11}$$

where $B = \text{bldiag}(F_{2D}, F_{2D}, \cdots, F_{2D})$ with F_{2D} being the matrix representing the 2D DFT whose size is $(N_x \times N_y) \times (N_x \times N_y)$ and "bldiag" denoting the block diagonal matrix, $Q = [P_1 P_2 \cdots P_{N_z}]$ with $[P_l]_{m_1 m_2} = e^{ikl\Delta_z} e^{il\Delta_z\sqrt{k^2-m_1^2\Delta_k^2-m_2^2\Delta_k^2}}$; $[P_l]_{m_1 m_2}$ represents the element of the matrix P_l at the intersection of the row m_1 and the column m_2, and G_{2D} represents the 2D inverse DFT matrix. As discussed earlier, ignoring the non-linearity of Eqn. (10) caused by the squared field term *e*, the Gabor hologram measurement may be algebraically written as

$$g = 2\text{Re}\{\bar{g}\} = 2\text{Re}\{G_{2D}QBf\} = 2\text{Re}\{Hf\} + e + n, \tag{12}$$

where $g \in \mathbb{R}^{N_x \times N_y}$ represents the Gabor hologram from which the DC component is removed, $H_{ij} = [G_{2D}QB]_{ij}$, and *e* and *n* denote vectorized $|E(x,y)|^2$ and additive noise, respectively. The nonlinear term is traditionally removed using off-axis holography. As demonstrated below, however, this term may be eliminated algorithmically from Gabor data using decompressive inference. We discuss the effects of *e* in Sec. 5.

We remark that the elements of the measurement matrix *H* (e.g., see Eqn. (12)) in holography are complex valued. In contrast, the typical optical imaging modality provides only nonnegative values because the only observable are the intensities. Such nonnegativity constraints confine the measurement basis space to be only the nonnegative orthant, which limits the angles between the measurement basis vectors (the columns of *H*) and effectively makes the coherence values large. On the other hand, interferometric imaging modalities such as holography allow the measurement vectors to reside in the entire space as opposed to the nonnegative orthant by allowing for negative values in the measurement basis vectors. Such negative values may enable us to design a sensing system with a small coherence value. This advantage with holography for compressive sensing remains valid in Gabor holography because although the f and g may be assumed to be real, the elements of the multiplex encoder *H* are still complex valued. We also note that in other holography such as the Leith-Upatnieks holography [25], the f and g as well as *H* are, in general, all complex valued.

Prior to discussing experimental estimation of f from Eqn. (12), we briefly consider the spatial resolution expected in the reconstruction and a sparsity constraint to enable decompressive inference. Optical measurement over a finite aperture is bandlimited. The band volume is the support in the 3D Fourier space of $\eta(x',y',z')$ for sampling $E(x,y)$ over a finite aperture. Spatial resolution in imaging systems is assumed to be inversely proportional to the limits of the

#111469 - $15.00 USD Received 18 May 2009; revised 2 Jul 2009; accepted 5 Jul 2009; published 15 Jul 2009

band volume, which yields transverse resolution $\Delta_x = \lambda z/D$ for objects at range z observed over aperture D and the axial resolution is $\Delta_z = \lambda(2z)^2/D^2$ [28]. Our objective is to achieve this resolution over the 3D datacube using decompressive inference of a 2D hologram.

If the entire diffraction pattern is captured by the hologram, the effective aperture size D for a Gabor hologram observed in the Fresnel diffraction zone is determined by size of the object feature observed. A feature of cross section w produces a diffraction pattern with cross section $D \approx \lambda z/w$. This implies that $\Delta_x \approx w$ and $\Delta_z \approx 4w^2/\lambda$. The dependence of axial resolution on feature size is the result of the "missing cone" in the paraxial band volume [28]. The missing cone may be removed by recording holograms along multiple axes. In the experiments described here, however, we are satisfied with the single axis band limited resolution. We anticipate, for example, that object features of approximately 100μ cross section will be observed under visible light with approximately 1 cm axial resolution.

Forward models such as Eqn. (12) have been inverted by decompressive inference by either selecting a basis, typically a particular wavelet basis, on which f may be assumed to be sparse or by enforcing a sparsity constraint on the total variation, as defined by Rudin *et al* [29], of f. We choose the second approach here and estimate f as

$$\hat{f} = \arg\min_f ||f||_{TV} \text{ such that } g = Hf, \tag{13}$$

where $\|f\|_{TV}$ is defined by

$$\|f_k\|_{TV} = \sum_k \sum_{n_1} \sum_{n_2} |\nabla(f_k)_{n_1,n_2}|, \tag{14}$$

where f_k denotes a 2D plane of the 3D object datacube. We adapt the two-step iterative shrinkage/thresholding algorithm (TwIST) [30] to solve this optimization problem.

4. Experimental results

The light scattered from the object and the collimated beam, which served as the reference beam, overlapped on a Lumenera LU100 1280×1040 pixel focal plane array with pixel pitch of 5.2 μm. We cropped the array of measurements to a 1024×1024 array, which is then downsampled to a 512×512 array using B-spline functions. The hologram, which is the interference pattern produced on the sensor, was digitized with 10 bits accuracy. The measurement vector g is then zero-padded on all four sides to create a 712×712 array to avoid the artifact of the circular convolution caused by using FFT. For our simulations, the matrix H has the size of $(712 \times 712) \times (712 \times 712 \times 10)$ with 10 being the number of object planes that can be changed by adjusting the related parameter. The reconstruction was performed on a digital computer with Intel Core2 Quad CPU Q9300 at 2.5 GHz and 8 GB of RAM. The data processing takes about 4 hours for H with the size of $(712 \times 712) \times (712 \times 712 \times 10)$. The codes were written in Matlab 7.7.

As illustrated in Fig. 2, we illuminated two seed parachutes of common dandelions (*taraxacum*) with a collimated, spatially filtered Helium-Neon laser of 632.8 nm wavelength. One object is placed 1.5 cm away from the detector array, and the other dandelion is placed 5.5 cm away from the detector array. Figures 3(b) and 3(c) are photographs of the two seed parachutes. The illumination and scattered fields were captured in the Gabor hologram shown in Fig. 3(a). Figure 3(d) is the 3D datacube estimated from the Gabor recording by the TV-minimization algorithm. As the reconstruction shows, the stem and the petals, representing the high-frequency features in the image, are reconstructed well. In addition, the distance between the detector plane and the first parachute and the distance between the two parachutes are also accurately estimated. We notice that there are still some errors in some reconstruction planes including the

#111469 - $15.00 USD Received 18 May 2009; revised 2 Jul 2009; accepted 5 Jul 2009; published 15 Jul 2009

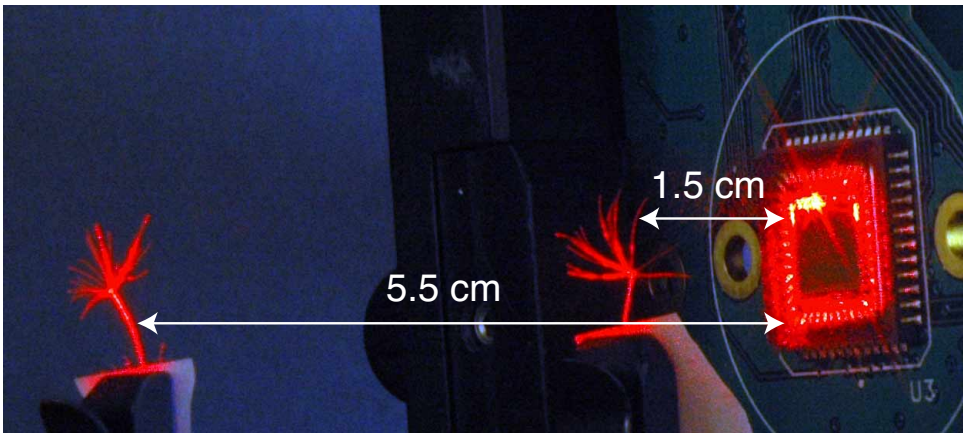

Fig. 2. Experimental apparatus.

planes in which the two seed parachutes. We conjecture that the errors are mainly reconstruction errors and the effects of noise, and they occur because of the rather insufficient number of measurements. The reconstruction errors can be suppressed by exploiting the phase-shifting holography that can increase the effective SNR and the effective number of measurements [31]. The reconstruction error in the plane of $z = 0$ is explained in Sec. 5. Figure 3(e) shows the backpropagated (or digital refocusing) field that is obtained by digitally backpropagating the hologram using the propagation kernel h in Eqn. (8) [25]. In contrast to the reconstruction in Fig. 3(d), the backpropagated field shows messy planes full of out-of-focus features obscuring the object features of the two parachutes.

5. Discussion

To understand the effects of the squared field $e(x,y)$ on the reconstruction, we consider the behavior of the algorithm. The algorithm determines how much portion of the measurement (or measurement estimate) should be placed in which object plane based on the amount of correlation that the diffraction patterns of the measurement and the diffraction pattern that the estimate at a particular object plane would produce. The squared field e is inclined to produce the diffraction patterns that bear little correlation with all of the object planes. Consequently, most of the reconstruction error caused by e tends to remain in the plane of $z = 0$. In this way, we may effectively isolate most of the errors that result from the squared field term. Since these errors are concentrated in the plane of $z = 0$ (measurement plane), such reconstruction values are not part of the object scattering density η by definition. Therefore, we may effectively remove most of the errors that would result from the squared field (zero-order) term in the reconstructions.

To verify this, we present two simple simulation examples: Figure 4(a) shows the reconstruction from a simulated squared field e, a rectangle with no diffraction patterns. As expected, all the signal e remains in the plane of $z = 0$ since the there is no information pertaining to which plane it diffracts from, meaning that the correlation of e with any object plane is small. In Fig. 4(b) , we simulated a 3D object that has two rectangles in the second and third planes from which the simulated squared field e is generated; the reconstruction is produced from only e without the field E. As the reconstruction illustrates, the reconstruction contains a small error in some object planes induced by little correlation between e and the interference patterns that the estimated object would produce. Otherwise, most of the errors are concentrated in the first

#111469 - $15.00 USD Received 18 May 2009; revised 2 Jul 2009; accepted 5 Jul 2009; published 15 Jul 2009

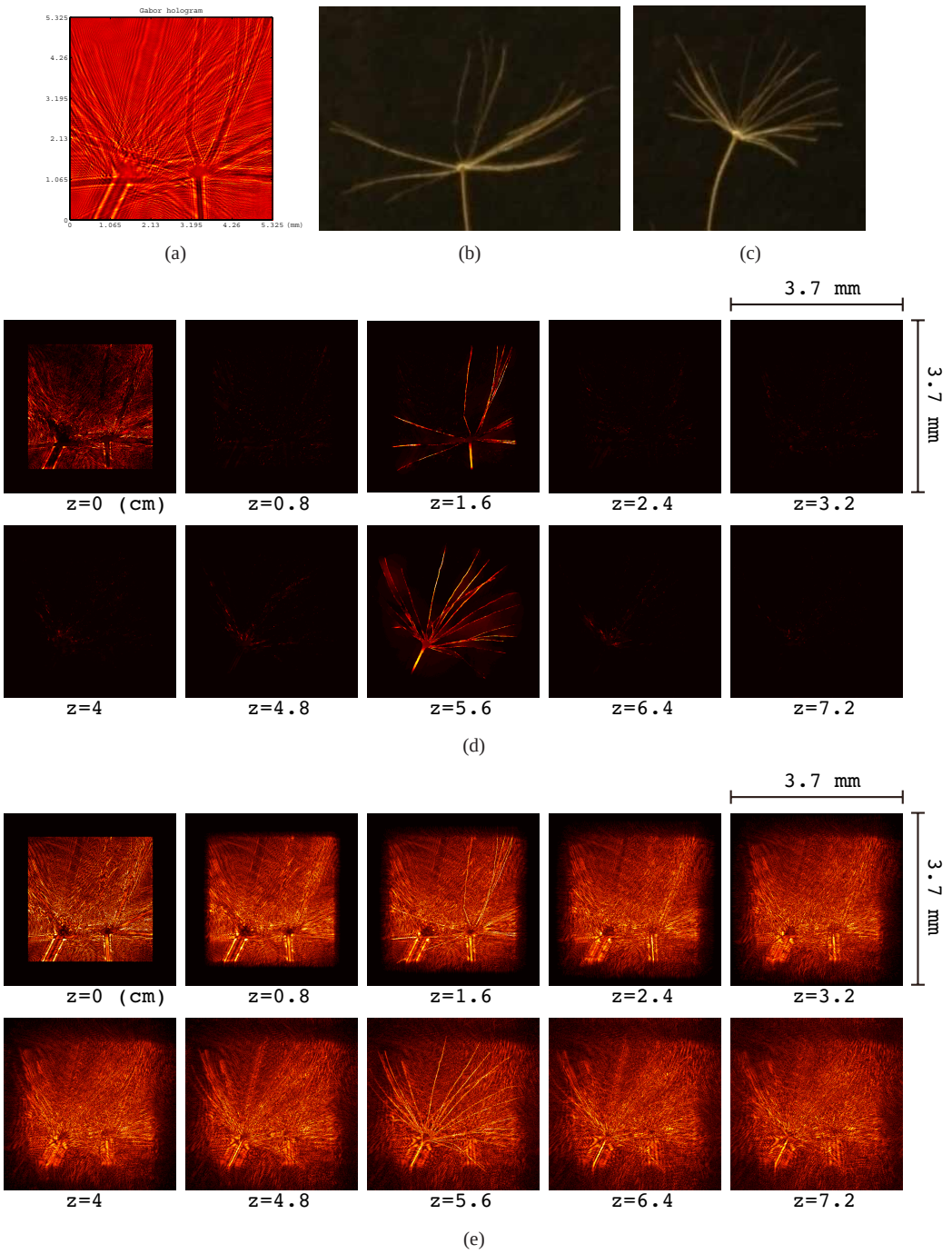

Fig. 3. (a) Raw Gabor hologram for seed parachutes of taraxacum arranged as in Fig. 2, (b) and (c) photographs of the individual objects, (d) transverse slices at various ranges of the tomographic reconstruction of the 3D data volume containing both objects, and (e) transverse slices at various ranges of the backpropagated (numerical refocusing) field.

#111469 - $15.00 USD Received 18 May 2009; revised 2 Jul 2009; accepted 5 Jul 2009; published 15 Jul 2009

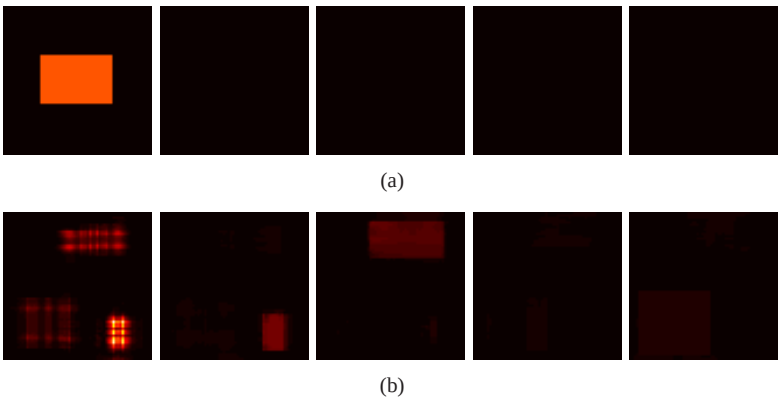

Fig. 4. Simulations showing the effects of squared field term e: the 3D datacube estimates from the squared field with no diffraction (a) and the squared field with diffraction (b).

plane ($z = 0$). Both cases imply that most of the errors produced by the squared field term in Gabor holography may be numerically isolated and effectively removed since they are related to the object scattering density.

Now, we consider the effects of the conjugate term $E^*(x,y)$ on the reconstruction. In conventional digital holography, the effect of the conjugate term on reconstructions is called the twin image problem [25]. Considering that e would behave as discussed above, our forward model including the conjugated field $E^*(x,y)$ is approximated well to be linear. In our approach, the effect of the conjugate term on the reconstruction can be numerically eliminated by confining our estimate domain to only the one side of the measurement plane (i.e., $z \geq 0$). Our decompressive inference method directly reconstructs the 3D volume object η rather than the field at a distance which is a superposition of all the object planes each of which is at a different focus. This implies that the virtual object η^* is placed to the other side of the measurement plane (i.e., $z \leq 0$) by our inference method. This aspect of our decompressive inference allows a separation of the real and the virtual objects. Hence, by confining the reconstruction domain to be the region in which $z \geq 0$, we can readily resolve the twin image problem in the reconstruction. A similar philosophy has successfully been applied to 2D holographic reconstruction to remove the twin image problem [32].

In conclusion, our results show that we can obtain a 3D ($512 \times 512 \times 10$, or $712 \times 712 \times 10$ after preprocessing to avoid the circular convolution effect) datacube of voxels with 5.2 μm transverse resolution and 0.8 cm axial resolution reconstructed from a single 2D (512×512) hologram. This demonstrates the main advantages of compressive holography, i.e. that holograms naturally encode high quality multiplex data and that decompressive inference can infer multidimensional objects from lower dimensional data. Extensions of compressive holography may use off-axis encoding to filter nonlinear terms and multispectral illumination to increase the band volume and improve axial resolution. It would be also useful to combine our approach with phase-shifting digital holography.

Acknowledgments

This research was supported by a DARPA under AFOSR contract FA9550-06-1-0230. The authors also thank the anonymous reviewers for their insightful comments and suggestions that significantly improve and help clarify this paper.

#111469 - $15.00 USD Received 18 May 2009; revised 2 Jul 2009; accepted 5 Jul 2009; published 15 Jul 2009